Dished Accelerator Grids on a 30-cm Ion Thruster

V. K. RAWLIN,* B. A. BANKS,† AND D. C. BYERS‡
NASA Lewis Research Center, Cleveland, Ohio

Several closely-spaced dished accelerator grid systems have been fabricated and tested on a 30-cm-diam Hg bombardment thruster and they appear to be a solution to the stringent requirements imposed by the near-term, high-thrust, low-specific impulse electric propulsion missions. The grids were simultaneously hydroformed and then simultaneously stress relieved. The ion extraction capability and discharge chamber performance were studied as the total accelerating voltage, the ratio of net-to-total voltage, grid spacing, and dish direction were varied.

Nomenclature

D_s = diameter of screen grid hole, cm
E_I = discharge energy per beam ion, ev/ion
h = grid dish depth, cm
J_A = accelerator current, ma
J_B = ion beam current, amp
j = beam current density, amp/cm^2
l = ion acceleration distance, grid spacing plus screen grid thickness, cm
l_g = grid-to-grid spacing, cm
Δl = change in ion acceleration distance, cm
P_B = ion beam power, kw
R = ratio of net to total ion accelerating voltage
R_g = radius of curvature of dished grid, cm
R_r = radius of grid mounting or half chord length of dished grid, cm
r = radial distance from beam axis to any point on grid, cm
S = arc length of dished grid, cm
T = thrust of ion engine, newton
ΔT_g = mean temperature increase of grid, °C
ΔT_r = mean temperature increase of mounting ring, °C
v = ion velocity, m/sec
Δz = change center of curvature of grid before and during operation, cm
α = coefficient of thermal expansion, °C^{-1}
β = angle between hot and cold radii of curvature at some point on grid, radians
γ = angle between thruster axis and any point on grid, radians
γ_{max} = maximum angle of dish, radians
η_u = propellant utilization efficiency
θ = azimuthal angle defining position of r, radians
λ = beam deflection angle due to grid hole misalinement, radians

Superscript

$'$ = prime denoting grid dimensions at room temperature prior to operation

Subscripts

A = accelerator grid
S = screen grid

Introduction

THE electron-bombardment ion thruster is being considered for a variety of space missions for which the optimum specific impulse is between 2000 and 3000 sec.[1,2] Such values of specific impulse have been obtained with thrusters using composite grids.[3–6] However, recent data indicate that satisfactory operation of composite grids is dependent on backsputtered facility material.[6] For this reason, it is probable that conventional two-grid accelerator systems will be required for near term missions. Achievement of specific impulses of 2000–3000 sec with two-grid systems at the desired thrust densities and thruster efficiencies requires essentially the following: 1) the screen grid be less than 0.5 mm thick, 2) the screen grid have a high open area fraction, preferably in excess of 0.7, and 3) a grid-to-grid spacing of approximately 0.25–0.75 mm be maintained over the entire grid system. Any practical ion extraction system must also survive both the launch environment and repeated thermal cycling. These factors combine to impose a difficult mechanical design problem. Techniques such as holding the grids in tension, supporting the screen grid from the Hg vapor distributor manifold, adding stiffener ribs, and interelectrode supports have been tested and/or proposed to solve the design problem.[5,7] This paper presents the experimental results concerning the fabrication and operation of dished grids on a 30-cm diam ion thruster.

Calculations are also made concerning the deflection of dished grids under thermal loading and thrust losses arising from the spherical shape of the grids.

Apparatus and Procedure

Dished Grid Fabrication

Many of the procedural details required for the successful fabrication of dished grids are given in Ref. 8. Therefore, only a brief summary will be given here. The screen and accelerator grids were first riveted together around the perimeter, then placed over a rubber sheet (Fig. 1). The grids were simultaneously hydroformed and then simultaneously stress relieved in an inert atmosphere. The resulting grids (Fig. 2) all had a dish depth h' of 2.54 cm and dish diam $2R_r'$ of 33.8 cm.

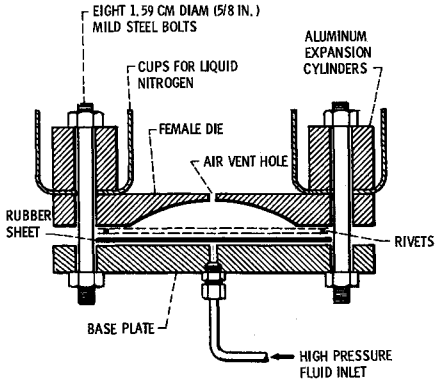

Fig. 1 Hydroforming apparatus.

Presented as Paper 72-486 at the AIAA 9th Electric Propulsion Conference, Bethesda, Md., April 17–19, 1972; submitted May 4, 1972; revision received August 10, 1972.

Index categories: Spacecraft Mission Studies and Economics; Electric and Advanced Space Propulsion.

* Aerospace Research Engineer, Spacecraft Technology Division, Ion Physics Branch, Propulsion Systems Section.

† Aerospace Research Engineer, Spacecraft Technology Division, Ion Physics Branch, Propulsion Components Section.

‡ Aerospace Research Engineer, Spacecraft Technology Division, Ion Physics Branch, Propulsion Systems Section. Member AIAA.

Table 1 Dished grid geometries

Grid set	Grid	Etch Ref. 8	Minimum hole diam	Equivalent percent open area	Maximum hole diam (on upstream surface), mm	Equivalent percent open area	Hole center-to-center spacing, mm
A	screen	50–50	1.9	51.0	2.0	58.0	2.54
	accelerator	50–50	1.9	51.0	2.0	58.0	
B	screen	90–10	1.9	51.0	2.3	73.4	2.54
	accelerator	50–50	1.9	51.0	2.0	58.0	
C	screen	50–50	1.2	48.5	1.4	58.9	1.71
	accelerator	90–10	1.2	48.5	1.5	70.3	

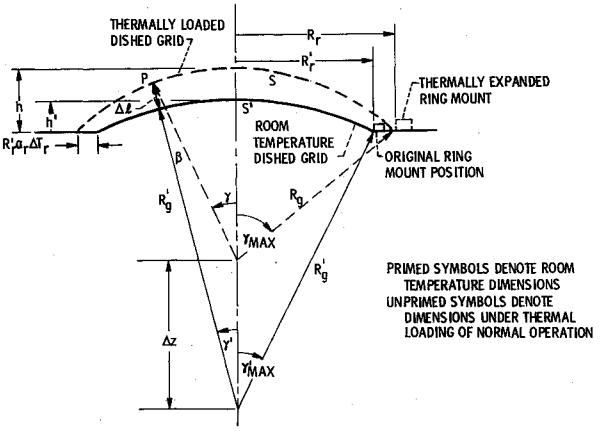

Fig. 2 Model used for grid deflection calculations.

The three grid sets reported in this paper were fabricated from a 0.38-mm-thick arc cast sheet of perforated Mo. The grid holes were produced in a hexagonal array over the entire Mo sheet by photochemical etching. Table 1 lists the hole dimensions and the percent open area for the various grid geometries tested.

To set a gap between the grids, they were first separated by insulating spacers of synthetic mica of glass and were later mounted on Mo rings.[8] The grid sets were mounted on the thruster with the dish direction both cancave and convex.

Thruster and Facility

A 30-cm-diam thruster, previously optimized for use with composite grids, was used to evaluate the dished two-grid accelerator systems. The thruster was built by Hughes Research Laboratories under contract NAS3-11523[5] and was used to obtain all the data presented herein.

The Hg flow rates reported were obtained with flow tubes, were repeatable to 1%, and were estimated to be accurate to within 2%. The thruster was operated in the 3.0-m-diam port of the 7.6-m-diam by 21.4-m-long vacuum tank at the Lewis Research Center.[9] The bell jar pressure during thruster operation was about 3×10^{-6} torr while the main tank pressure was 2×10^{-7} torr.

Accelerator Grid Evaluation

Data were taken to determine the minimum total voltage between the grids at a given beam current which would not lead to accelerator impingement currents greater than 2–3% of the beam current. This method, which was similar to that used by Kerslake,[10,11] was used consistently to evaluate each grid set relative to other grid sets. Also each grid set was checked, at various levels of beam current and net accelerating voltage, for the value of accelerator grid voltage at which electron backstreaming occurred.

The grid-to-grid spacing was measured before and after a test by inserting L-shaped wires of various diameters into the grid holes. The grid spacings were also measured by intruding a dental impression material into the grid holes and between the grids. After the dental material cured, the grids were separated, the spacing impression was removed, and a photomicrograph was taken. The cold grid-to-grid spacings measurements are estimated to be accurate within 0.05 mm.

Results and Discussion

Operation of Dished Two-Grid Accelerator Systems

Dished grids have been fabricated and operated on a 30-cm thruster over a large range of test conditions. The grid voltages, spacings, dish direction, and hole diameters have been varied and found to affect the thruster performance. An attempt will be made to separate and discuss these parameters and their effects.

Some geometric properties of the grid sets tested are listed in Table 2. Grids with minimum hole diameters of 1.2 and 1.9 mm were tested. The cold (room temperature) grid-to-grid spacing was varied from 0.30 mm to 0.86 mm. The grids were operated both convex and concave.

Dished grid perveance

Figure 3 is a plot of the minimum total (or knee) voltages at the corresponding beam currents for the six grid sets tested. The shaded portion of Fig. 3 shows the region of composite grid operation from Refs. 4 and 5. The data of Fig. 3 shows an increase in perveance per unit of about 4.0 times over the previous maximums reported for bombardment thrusters greater than

Table 2 Grid spacing and performance

Test number	Table 1 grid design	Dish direction	Cold grid spacing, mm	Estimated ion acceleration distance mm	Knee voltage for beam current of: 0.7 amp	1.0 amp	1.5 amp	2.0 amp	2.5 amp	3.0 amp
1	A	convex	0.66	0.78	630 v	720 v	830 v	1010 v	1090 v	...
2	A	convex	0.86	0.98	740	...	980	1140	1260	1420
3	A	concave	0.86	1.50	920	1040	1290	1550	...	...
4	A	concave	0.33	0.97	720	850	980	1160	...	...
5	B	convex	0.86	0.98	740	840	980	1140	1260	1420
6	C	concave	0.30	0.94	820	960	1220	1330	1500	...

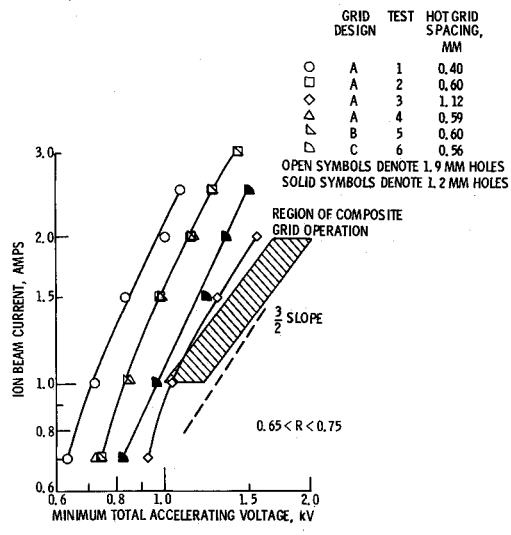

Fig. 3 Ion beam current as a function of minimum total accelerating voltage for grid sets of Table 2.

15-cm-diam with conventional two-grid optics.[12,13] This increase is due to the small grid spacing that can be stably maintained with the dished grids.

Because all the dished grids reported herein had approximately the same effective open area, the primary cause for the different perveance was the different ion accelerating distance of each grid set.

Figure 3 shows that the beam current extracted by each grid set increased with voltage but at a power greater than the three-halves predicted by Child's law. This could occur if the plasma density profile varied as the thruster conditions were changed at higher beam currents. The actual beam currents shown in Fig. 3 are only 20–60% of the ideal beam current predicted by Child's law when the sum of the hot grid spacing and the screen grid thickness is used for the ion acceleration distance. The experimental perveance is probably less than ideal because 1) the plasma density is not uniform across the grid, and 2) at the grid spacing to hole diameter ratios used herein, the grid aperture effect[10] predicts reductions of the ideal beam current between 35 and 55%.

The data presented in Fig. 3 show that a thruster with dished grid meets the performance requirements of near term, high-thrust, low-specific impulse missions.

Grid-to-grid spacing

The perveance for the grid sets of test 2 and 4 are shown in Table 2 and Fig. 3. For test 2 the grids were mounted convex downstream and the cold grid spacing was 0.86 mm. For test 4 the grids were mounted concave with a spacing of 0.33 mm. When operated, the perveance of grids of test 2 was identical to that of test 4. During operation, the screen grid was hotter than the accelerator grid and underwent the most deflection; therefore, the spacings of the grids decreased for test 2 and increased for test 4. The change in spacing during operation for the grids of test 2 and 4 was estimated by assuming that 1) two sets of grids having the same extraction hole geometry and perveance must also have the same effective ion accelerating distance; and 2) under identical thermal loading, the grid deflection is independent of the grid dish direction.

The change in spacing was expected to be about one-half the difference of the cold spacing, or 0.26 mm. This gave a hot grid-to-grid spacing of 0.60 mm for each test. This spacing variation is in good agreement with the calculated values presented later in the paper.

Figure 4 is a plot of the beam currents from Fig. 3 at a constant total voltage of 1000 v as a function of l, the ion accelerating distance. The distance l was calculated as the sum

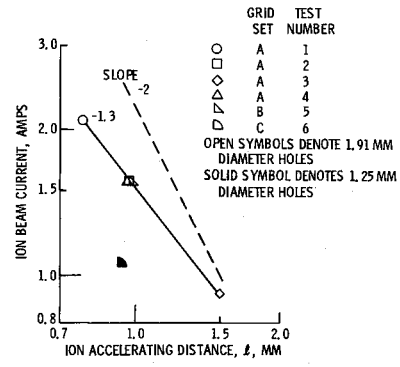

Fig. 4 Ion beam current as a function of estimated hot spacing for several grid sets at a total voltage of 1 kV.

of the cold spacing, the 0.38-mm screen grid thickness, and the positive or negative 0.26-mm estimated change in spacing during operation.

Figure 4 shows that the beam current increased as l was decreased. The slope of the line drawn through the data for the grids with 1.9 mm diam holes is -1.3 rather than -2 as expected from Child's law. Again, probable reasons for the reduced experimental beam currents are the nonuniform plasma density profile and the grid aperature effect.

In test 2 the discharge power was varied from 200 to 500 w at a beam current of 1.0 amp. The minimum value of total voltage was not changed by this variation of thermal loading.

Ratio of net-to-total voltage

At a fixed total voltage and beam current, the specific impulse of the thruster can be varied, within limits, by changing the ratio of the net-to-total voltage, R. Figure 5 shows how the ratio of accelerator impingement current to beam current J_A/J_B changed as R was varied. The upper curve, where J_A/J_B was sensitive to R, resulted when the accelerator grid mount was large in size and exposed to the downstream plasma. The range of low J_A/J_B was extended to approximately 0.4 by shielding the large area of material at accelerator potential. At values of R less than 0.4, the rise in J_A/J_B was probably due to overfocused beam ions.

Grid hole diameter and etch

Grids with hole diameters of 1.2 and 1.9 mm were tested. The fraction open area of all grids tested was about 0.50. Preliminary results, shown in Figs. 3 and 4 have indicated a loss in the grid extraction capability when the hole size was decreased from 1.9 to 1.2-mm-diam for a constant spacing. Further testing would be required to determine the optimum hole diameter for closely spaced 30-cm grids.

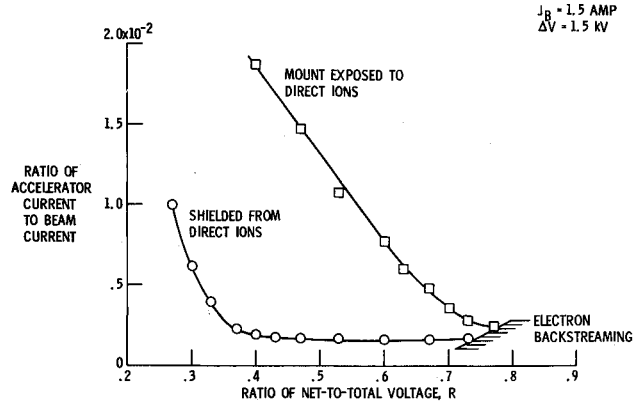

Fig. 5 Effect of downstream accelerator grid mount geometry on R ratio sensitivity for dished grids.

In order to determine the effect, if any, of the grid etch on grid perveance, tests 2 and 5 were conducted. In test 2, both grids had a 50-50 etch while in test 5, the screen grid had a 90-10 etch and the accelerator has a 50-50 etch. The grids of tests 2 and 5 had equal cold spacings of 0.86 mm and were dished convex. As shown in Fig. 4 and Table 2, the perveance was identical for both grid sets.

Electron backstreaming

During the operation of dished grids, the electron backstreaming limit of the accelerator voltage was found to be a function of the beam current, accelerator grid hole diameter, net accelerating voltage R and grid spacing. Figure 6 shows the effect of the value of beam current and the accelerator grid hole diameter on the electron backstreaming limit. The absolute value of the accelerator voltage backstreaming limit increases approximately linearly with beam current. The scatter in the data for grids with 1.9-mm-diam holes is largely due to the wide range of net accelerating voltages used—from 300 to 1200 v. The backstreaming limit for the grids with 1.2-mm-diam holes was roughly 40% of that required for the larger 1.9-mm holes.

The Effects of Dished Grids on Discharge Chamber Performance

References 3–5, 14, and 15 have shown that the ion extraction system affects the thruster discharge chamber performance. This section presents similar results showing the effect of grid system parameters such as grid type, voltages, and dish direction on the discharge chamber performance.

Grid type and voltage

Figure 7 is a plot of the discharge energy per beam ion E_I as a function of the propellant utilization efficiency η_u for 30-cm thrusters with several different accelerator grid systems. The E_I of the thruster with the present dished grids was about 325 at a η_u of 90% whereas the E_I with composite grids was about 170.[4,5] This increase in E_I was probably due to the decrease in the fraction open area of the dished grids (51%) from the effective value for composite grids (estimated to be >90%[4]). Preliminary tests with high open area (67%) dished grids have lowered the base level E_I to about 150 ev/ion. In addition, it was also found that as the total accelerating voltage was lowered, the discharge losses increased. For example, at a beam current of 1.5 amp, the total voltage was lowered from 1600 to 1400 v at a constant R. At an η_u of 86% E_I increased by about 25. This degradation was probably the result of the plasma sheath at the screen grid moving away from the discharge chamber as the total voltage was lowered and creating a smaller effective grid open area.[14]

Direction of grid dish

Figure 8 is a plot of E_I vs η_u for tests 2 and 3 of Table 2 where the cold grid spacings were identical but the dish directions were opposite. The data were obtained at a beam

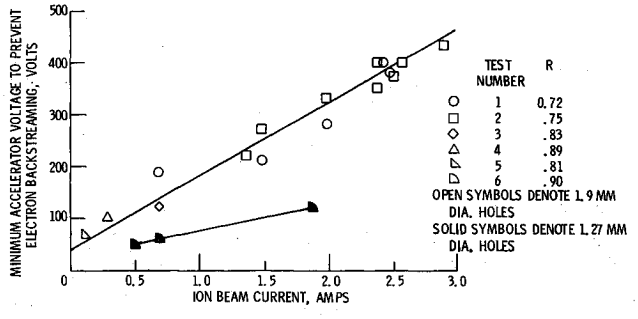

Fig. 6 Electron backstreaming limit of accelerator voltage as a function of beam current for several grid sets.

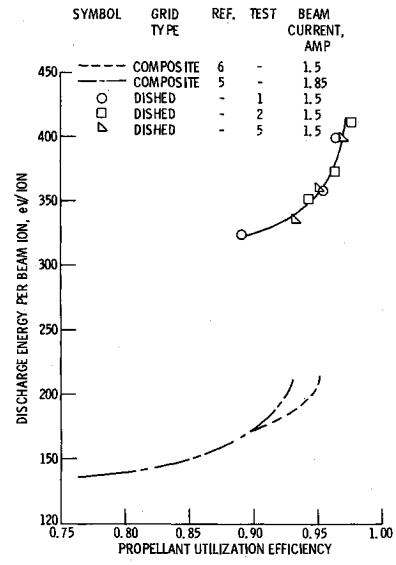

Fig. 7 Discharge chamber performance with composite grids and dished grids.

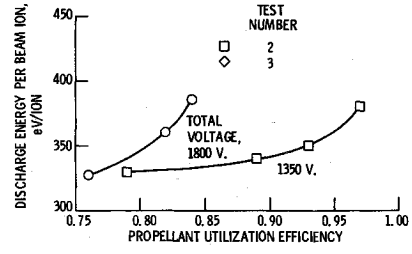

Fig. 8 Discharge chamber performance for grids with same cold spacing and different dish directions, $J_B = 2.0$ A.

current of 2.0 amp. The total accelerating voltages necessary to operate about 200 v above the knee were 1350 and 1800 v for tests 2 and 3, respectively.

As shown previously, operation at lower total voltage degraded discharge chamber performance. However, it is shown in Fig. 8 that an E_I of 350, the η_u of test 2 was 12% higher than test 3. This occurred even though test 2 was operated at a total voltage 450 v less than test 3. This effect was probably due to the decreased hot spacing for the convex grids of test 2 and the increased hot spacing for the concave grids of test 3. Reference 14 has also shown that E_I increased as the grid spacing was increased.

Theoretical Analysis

Grid Deflection

A brief calculation was made of the deflection of dished grids under thermal loading. Because data presented herein were obtained with grids without intermediate grid supports, the analysis of deflection will be for grids supported only on the edges. It was assumed that the shapes of the screen and accelerator grids were spherical before operation. It was assumed that the radii of curvature of both grids were equal. Figure 2 shows the model used for the calculations.

Present tests indicate that during operation the center of the screen grid heats up to between 350–500°C and the center of the accelerator grid to a somewhat lower temperature. Thermal gradients of 350°C could exist between the center of the grids and the ring support. Because the supports are cooler than the grids, the grids deflect by an amount Δl which depends on the average temperature of the grid and the temperature of the ring support. It was assumed that the new shapes, shown by the

dotted line on Fig. 2, were also spherical. The screen grid was the hotter of the two grids and underwent the most deflection.

The intent of the following calculation is to determine the grid-to-grid spacing variation for various geometries and operating conditions. The variation of spacing is defined as the net difference between the deflection of each grid during operation.

The known dimensions are the dish depth h' and a half chord length R_r'. The grid has a radius of curvature R_g' given by

$$R_g' = (R_r'^2 + h'^2)/2h' \quad (1)$$

From Fig. 2 it can be seen that the deflection of a single grid Δl, which is measured along an extension of the initial radius of curvature to point P can be obtained from the equation

$$(R_g' + \Delta l)\sin\gamma = \Delta z/\sin\beta \quad (2)$$

Details of the derivation can be found in Ref. 8. The grid-to-grid spacing variation can be calculated by substituting values of the mean temperature increase of each grid and mounting ring into the appropriate equation. Substitution of various values of h' into Eq. (1) can show the effect of various values of dish depth. Figure 9 shows the calculated variation of grid-to-grid spacing of a grid set during operation for several values of dish depth and an initial value of R_r' of 15 cm. The temperature increases ΔT_{rS} and ΔT_{rA} of the screen and accelerator mounting rings were assumed equal to 170°C. The average temperature increase, from room temperature, of the screen grid ΔT_{gS} was assumed to be 400°C, and the average temperature increase of the accelerator grid ΔT_{gA} was assumed to be 300°C.

The grid-to-grid spacing variation is maximum at the center of the grid and falls to zero at the edge of the grid system. For the conditions assumed for Fig. 9, the maximum change in spacing for a 2.54-cm dish, which was used for all performance data presented herein, was about 0.36 mm. When an average temperature increase of 350°C (instead of 300°C) for the accelerator grid was assumed, the maximum variation in grid-to-grid spacing was 0.18 mm. The 0.36 and 0.18-mm maximum variations in the calculated grid-to-grid spacing are in approximate agreement with the 0.26-mm average variation estimate obtained from the grid.

The change in spacing is a strong function of the initial dish depth. For example, the calculated value of the maximum change in spacing decreased by about a factor of 2.5 as the chosen initial dish depth increased from 1.27 to 3.81 cm.

The data of Fig. 9 indicate that to minimize the grid-to-grid spacing variation during operation, it is desirable to fabricate the grids with as deep a dish as possible. On the other hand, the thrust losses increase as the dish depth increases.

Thrust losses from hole misalinement

The present technique of dishing grids with identical hole patterns leads to a grid hole misalinement which is a function of γ. Figure 10a is a section view of the grids after dishing and stress relieving. Figure 10b shows the same set of grids during operation with the grids mounted convex. Figure 10b also shows that there is a grid hole misalinement (maximum at the outer holes) caused by the grid-to-grid spacing separation.

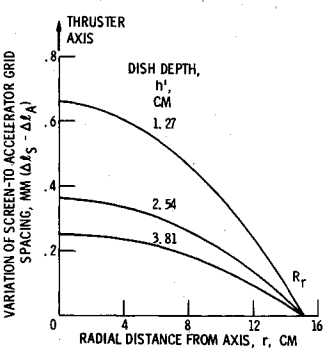

Fig. 9 Screen-to-accelerator grid spacing variation during operation, R_r', 15 cm; $\Delta T_{gs}=400$°C, $\Delta T_{gA}=300$°C.

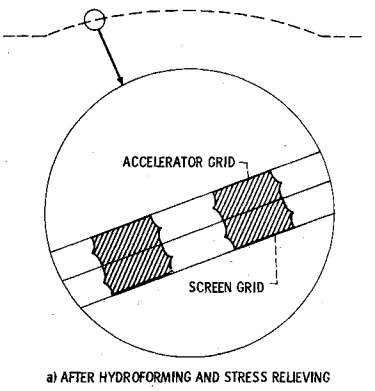

a) AFTER HYDROFORMING AND STRESS RELIEVING

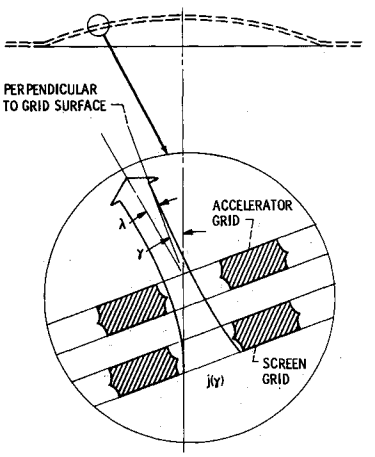

b) AFTER SETTING GRID SPACING AND DURING OPERATION

Fig. 10 Section views of dished grids.

The current density extracted at the screen grid at element dA and at an angle γ from the thruster axis is defined as $j(\gamma)$. Each beamlet is deflected by γ due to the shape of the grid. The grid hole misalinement leads to an additional beam deflection λ which is a function of γ. The following section will present calculations to determine the effect of dishing on the thrust to beam power ratio. This is a measure of the thrust loss due to ion beam divergence from the grid set as assembled. It is beyond the scope of this report to determine analytically beam deflections due to grid distortions during operation. Such additional beam deflections may add or subtract to the thrust losses caused by the basic grid geometry.

The total axial thrust and beam power of a dished grid can be calculated by

$$T = \frac{R_g^2 mv}{q}\int_0^{2\pi} d\theta \int_0^{\bar{\gamma}} j(\gamma)\cos(\gamma+\lambda)\sin\gamma d\gamma \quad (3)$$

$$P_B = \frac{R_g^2 mv^2}{2q}\int_0^{2\pi} d\theta \int_0^{\bar{\gamma}} j(\gamma)\sin\gamma d\gamma \quad (4)$$

By assuming the form of the ion current density and making certain approximations, the thrust and beam power can be evaluated in closed integral form. Again, the details are given in Ref. 8.

The value of the thrust to beam power ratio for an ideal grid with no divergence loss is

$$(T/P_B)_{\text{ideal}} = 2/v \quad (5)$$

To normalize the divergence thrust loss, the values of thrust to beam power ratios calculated from Eqs. (3) and (4) are multiplied by the product $v/2$.

Figure 11 shows the normalized thrust to beam power ratio plotted as a function of grid depth for a 30-cm diam thruster. As explained in Ref. 16, the thrust loss is a function of the ratio of the cold grid spacing to hole diameter ratio l_g/D_S. Therefore, two values of l_g/DS, similar to those used experimentally, are shown. The case of no misalinement is also shown. In this

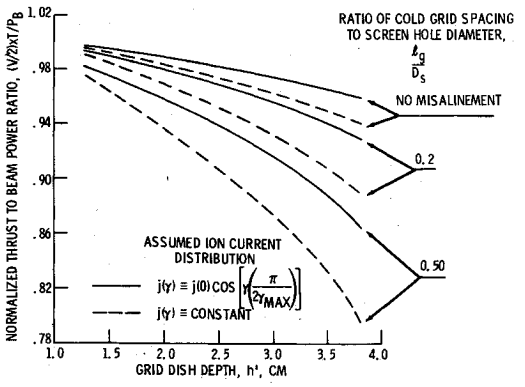

Fig. 11 Ratio of thrust to beam power as a function of grid dish depth, R_r', 15 cm.

case, the grids are assumed to be fabricated in such a fashion as to allow the ions to be ejected normal to the grid surface and the thrust loss is due only to the spherical shape of the grid surface.

For convenience it will be assumed that the actual thrust loss is midway between that predicted by use of the two different assumed ion current density profiles. Figure 11 shows that the thrust losses due to beam divergence increase with both the grid dish depth and the l_g/D_S ratio. The divergence loss for the case of no misalinement varies from approximately 0.5 to 5% as the dish depth increases frm 1.27 to 3.81 cm. For the case of misalined grid holes, the thrust loss increases strongly with the l_g/D_S ratio.

A dish depth of 2.54 cm and l_g/D_S ratios of 0.23 and 0.6 were used for the experimental data of this paper. For these grid geometries the estimated thrust losses were between 4 and 8%. Various techniques which could reduce the thrust losses are mentioned in Ref. 8.

Lifetests

As of Jan. 1, 1972, the set of grids used in tests 1–4 have accumulated 1365 hr of operation, including 700 hr at a beam current of 2.5 amp. This set of grids has been thermally cycled in 15 separate test segments with no change in the ion extraction capability. The thruster efficiencies (not optimized for minimum fixed power losses or neutralizer flow rate) are listed in Table 3. The total thruster efficiency increased from 0.60 to 0.64 and the specific impulse increased from 2620 to 2910 sec as the beam current was increased from 1.5 to 2.5 amp. The ideal thrust to power ratio was nearly constant at 46×10^{-6} N per w (10^{-2} lb/kw).

Table 3 Lifetest performance

Total hr at beam current below	25	375	200	700
Table 2 test number for data below	2	2	1	1
Beam current, amp	0.7	1.5	2.0	2.5
Net accelerating voltage, v	800	900	1000	1000
Accelerator current, amp	0.0015	0.004	0.006	0.008
Accelerator voltage, v	400	450	500	500
Emission current, amp	6.0	13.8	20.0	25.0
Discharge voltage, v	40	40	40	40
Fixed power loss, w	87	92	98	103
Total input power, w	890	2000	2907	3615
Power efficiency, η_P	0.63	0.68	0.69	0.69
Utilization efficiency, η_u	0.73	0.88	0.90	0.93
Total efficiency, η_T	0.46	0.60	0.62	0.64
Specific impulse, sec	2520	2620	2820	2910
Ideal thrust	0.041	0.093	0.131	0.164
Newton (mlb)	(9.2)	(21)	(58)	(73)
Ideal thrust to power ratio N/w $\times 10^6$	46	46	45	45

The familiar charge exchange ion erosion pattern on the downstream side of the accelerator was just barely visible. A plasma-bridge neutralizer, operating at 50–130 equivalent mA, was used for these tests and did not cause any measurable grid erosion. There was a slight erosion pattern on the grid near the neutralizer but the depth was less than the surface roughness. Based on the appearance of the grids after 1365 hr, the time to erode the grids to failure should be well in excess of 10,000 hr.

Conclusions

The methods and results of the fabrication and testing of dished grids on a 30-cm diam thruster have been presented. It was found necessary that the screen and accelerator be simultaneously hydroformed and then simultaneously stress relieved to provide matched contours of the two grids. Thus, when separated, the spacing was uniform over the entire grid surface. When heated to operating temperature, the dished design permitted a controlled thermal expansion of the grids which resulted in repeatable high values of grid perveance and thrust densities. These values are equal to or greater than those of the previously tested composite and two grid accelerator systems. Ion beam currents up to 3.0 amp have been obtained at net acceleration voltages from 500 to 1500 v. The beam current increased as the total voltage was increased or the grid spacing was decreased but not at the powers predicted by Child's law. The accelerator system perveance and discharge chamber performance improved when a given set of dished grids was mounted convex, as viewed from downstream of the thruster.

One of the grid sets tested has accumulated 1365 hr of operation, 700 of which have been at a beam current of 2.5 amp. There has been no significant erosion problems with the grids to date.

From these preliminary results, a closely-spaced, dished accelerator grid system appears to be a solution to the stringent requirements imposed by the near-term, high-thrust, low-specific impulse electric propulsion missions.

References

[1] Bartz, D. R. and Horsewood, J. L., "Characteristics, Capabilities, and Costs of Solar Electric Spacecraft for Planetary Missions," *Journal of Spacecraft and Rockets*, Vol. 7, No. 12, Dec. 1970, pp. 1379–1390.

[2] Strack, W. C. and Hrach, F. J., "Early Application of Solar-Electric Propulsion of a 1-Astronomical-Unit Out-of-the Ecliptic Mission," TN D-5996, 1970, NASA.

[3] Bechtel, R. T., "Performance and Control of a 30-Cm-Diam., Low-Impulse, Kaufman Thruster," *Journal of Spacecraft and Rockets*, Vol. 7, No. 1, Jan. 1970, pp. 21–25.

[4] Bechtel, R. T., "Component Testing of a 30-Centimeter Diameter Electron Bombardment Thruster," AIAA Paper 70-1100, New York, 1970.

[5] King, H. J. and Poeschel, R. L., "Low Specific Impulse Ion Engine," NASA CR-72677, Feb. 1970, Hughes Research Labs., Malibu, Calif.

[6] Bechtel, R. T., Banks, B. A., and Reynolds, T. W., "Effect of Facility Backsputtered Material on Performance of Glass-Coated Accelerator Grids for Kaufman Thrusters," AIAA Paper 71-156, New York, 1971.

[7] Pawlik, E. V., Costogue, E. N., Ferrera, J., and Macie, T. W., "Solar Electric Propulsion System Evaluation," *Journal of Spacecraft and Rockets*, Vol. 7, No. 8, Aug. 1970, pp. 968–976.

[8] Rawlin, V. K., Banks, B. A., and Byers, D. C., "Design, Fabrication, and Operation of Dished Accelerator Grids on a 30-Cm Ion Thruster," AIAA Paper 72-486, New York, 1972.

[9] Finke, R. C., Holmes, A. C., and Keller, T. A., "Space Environment Facility for Electric Propulsions Systems Research," TN D-2774, 1965, NASA.

[10] Kerslake, W. R. and Pawlik, E. V., "Additional Studies of Screen and Accelerator Grids for Electric-Bombardment Ion Thrusters," TN D-1411, 1963, NASA.

[11] Kerslake, W. R., "Charge-Exchange Effects on the Accelerator

Impingement of an Electron-Bombardment Ion Rocket," TN D-1657, 1963, NASA.

[12] King, H. J. et al., "Low Voltage 30-Cm Ion Thruster," NASA CR-120919, Feb. 1972, Hughes Research Labs., Malibu, Calif.

[13] Macie, T. W. et al., "Integration of a Flight Prototype Power Conditioner with a 20-Cm Ion Thruster," AIAA Paper 71-159, New York, 1971.

[14] Byers, D. C., "An Experimental Investigation of a High-Voltage Electron-Bombardment Ion Thruster," *Journal of the Electrochemical Society*, Vol. 116, No. 1, Jan. 1969, pp. 9–17.

[15] Bechtel, R. T., "Discharge Chamber Optimization of the SERT II Thruster," *Journal of Spacecraft and Rockets*, Vol. 5, No. 7, July 1968, pp. 795–800.

[16] Lathem, W. C. and Adam, W. B., "Theoretical Analysis of a Grid-Translation Beam Deflection System for a 30-Cm Diameter Kaufman Thruster," TM X-67911, 1971, NASA.

JANUARY 1973 J. SPACECRAFT VOL. 10, NO. 1

Ion Thruster Thermal Characteristics and Performance

L. WEN,* J. D. CROTTY,† AND E. V. PAWLIK‡
Jet Propulsion Laboratory, Pasadena, Calif.

Experimental and analytical results for a typical 20-cm-diam, hollow-cathode ion thruster are reported. The foundation of the investigation was the application of thermal model correction techniques. Pertinent thermal properties and plasma heating characteristics of the thruster were determined through correlation and integration of temperature measurement data with a single-state Wiener-Kalman filter. The thruster self-heating levels on various parts were realistically estimated. Analytically predicted temperatures were forced to agree with the measured values for the purpose of constructing a corrected thermal model, which could then be used to evaluate more realistic thruster circumstances and environments. The expected accuracy of the resultant analytical network model was demonstrated to be ±10 K. Thruster thermal performance data for a typical five-thruster array are presented as functions of environmental solar intensities. The thermal analyses are also extended to a 30-cm thruster system.

Nomenclature

A = thermal radiation surface area, cm^2
b_{jk} = the (j, k)th element of the matrix $[\mathbf{B} + \mathbf{HPH}^T]^{-1}$
$\mathbf{C}$ = a diagonal matrix with elements c_k^2
c_k = uncertainty limit of parameter v_k
$\mathbf{D}$ = a diagonal matrix with elements $(\Delta T_m)^2$
$\mathbf{E}$ = covariance matrix of vector $\mathbf{R}$
e_m = expected random error in measurement m
$\mathscr{F}_{ij}$ = Hottel's script-F factor
$\hat{F}_{ij}$ = total radiation exchange factor, $\hat{F}_{ij} = \mathscr{F}_{ij}/\varepsilon_i\varepsilon_j$
H = a $M \times L$ matrix of sensitivity coefficients, $\partial T_i/\partial v_k$
K_{ij} = thermal conductance between nodes i and j
L = number of parameters to be determined
M = number of measurements
$\mathbf{P}$ = covariance matrix of vector $\mathbf{X}$
Q = net thermal energy input to node i
$\mathbf{R}$ = residual vector with elements $r_1, r_2, \ldots, r_m$
r_m = observation residual
s_k = the (k, k)th element of matrix $\mathbf{P}$
T = nodal equilibrium temperature
ΔT = deviation between measured data and calculated results
v = parameter to be determined
Δv = correction factor
$\mathbf{X}$ = a L-vector consisting of all correction factors
$\mathbf{Y}$ = a M-vector with elements ΔT_m
ε = total hemispherical emittance
σ = Stefan Boltzmann constant

Subscripts and superscripts

i = nodal value
j = integer
k = integer, parameter count
m = integer, measurement count
c = integer, measurement count
c = calculated value
$*$ = measured value
$\circ$ = nominal value
T = transpose of matrix

Received May 30, 1972; revision received September 18, 1972. This paper presents the results of one phase of research carried out at the Jet Propulsion Laboratory, California Institute of Technology, under Contract NAS 7-100, sponsored by NASA. The authors acknowledge the assistance of the Electric Propulsion Applications Laboratory staff of the Jet Propulsion Laboratory. The contributions to the instrumentation and test setups by E. Hopper were invaluable in obtaining the thruster temperatures.

Index categories: Electric and Advanced Space Propulsion; Thermal Modeling and Experimental Thermal Simulation.

* Senior Engineer. Member AIAA.
† Consultant.
‡ Member Technical Staff. Member AIAA.

Introduction

THE integration of a thruster array with a spacecraft requires a comprehensive understanding of their thermal interaction under various operating conditions. Some basic thruster thermal constraints include: 1) maintenance of vaporizer control at high temperatures; 2) prevention of freezing of the mercury propellant; 3) maintenance of cathode temperature in the proper range; and 4) maintenance of thruster housing temperatures below a limiting temperature to prevent overheating of magnets. Accurate thermal analysis is required in all stages of spacecraft development. It serves as a useful tool in evaluating thruster design configurations[1,2] and in predicting over-all spacecraft system performance.

The reliability of thermal analytical results is governed by the parameters describing the mathematical model. Detailed information about the following parameters has to be available prior to any meaningful thermal analysis of ion thrusters: 1) thermophysical properties of thruster components, such as thermal contact conductances, surface emittances, and material thermal conductivities; 2) thruster self-heating pattern due to electron, ion, and plasma radiation heating; 3) design configurations and arrangement of clustered arrays; and 4) environmental conditions, solar heating levels, and the thermal coupling between the thruster array and the spacecraft.

Because of the complexity of the design and the operating mode, accurate information on the self-heating distribution and